J|A|C|S ARTICLES

Published on Web 06/18/2010

Order at the Edge of the Bilayer: Membrane Remodeling at the Edge of a Planar Supported Bilayer Is Accompanied by a Localized Phase Change

Andreia M. Smith,[†] Madhuri Vinchurkar,[‡] Niels Gronbech-Jensen,[‡] and Atul N. Parikh*[,†,‡]

Biophysics Graduate Group, University of California, Davis, California 95616, and Department of Applied Science, University of California, Davis, California 95616

Received January 12, 2010; E-mail: anparikh@ucdavis.edu

Abstract: We present experimental evidence for the existence of a unique molecular-level order in the vicinity of the bilayer's edge. Discrete patches of substrate-supported lipid bilayers exhibiting stable edge defects are prepared by confining vesicle fusion to hydrophilic patches of a chemically patterned substrate exhibiting hydrophilic patches in hydrophobic surrounding, and edge properties are characterized by fluorescence and vibrational spectroscopy based measurements. Specifically, wide-field fluorescence microscopy using phase-sensitive dyes, temperature-programmed fluorescence recovery measurements, and temperature-dependent attenuated total reflection Fourier transform infrared spectroscopy measurements are performed to characterize the local chain conformational properties, local diffusional characteristics, and phase discrimination afforded by phase-sensitive DiI fluorescent probes. We find that the bilayer structure near the edge is characterized by (1) an increase in intramolecular conformational order; (2) reduced effective lateral mobility; and (3) a distinctly higher local, effective gel-fluid transition temperature in comparison to their bulk counterpart. Together, these features signal the emergence of unique ordering presumably triggered by the hemimicellar configuration of the edge. These results are consistent with simulations of lyso-lipid micelles predicting the presence of dynamic clusters of ordered lipids in comparable micellar topology and disagrees with some recent interpretations of mobility near the edges of supported bilayers. Our results also offer the structural basis for the stability of defects and edges in fluid supported bilayers, and may be relevant in understanding the ordering and stabilization of pores, edges, and defects generated in membrane bilayers by proteins, curvature-sensitive lipids, antimicrobial peptides, and detergents.

Introduction

Topological defects and discontinuities are rarely encountered in uniform lipid microphases which form via self-assembly in water.[1] Rather, aqueous suspensions of these amphiphiles reveal a rich variety of closed shapes and configurations (e.g., spheres, tubules, ellipsoids) determined by a combination of intrinsic (e.g., spontaneous curvature) and experimental (e.g., concentration and temperature) conditions. The formation of such defect-free, dynamic lipid aggregates reflects the preponderance of the so-called hydrophobic effect,[2] which relates to energetic penalties of exposing the hydrophobic lipid-tails to the aqueous environment, and high edge-energies associated with the formation of defects.[3] Indeed, a simple energetic balance between the reduction in membrane tension energy, $-\pi R^2\sigma$ (σ is membrane tension), and the line-tension penalties, $+2\pi R\gamma$ (γ represents line tension), associated with creating a defect of dimension R within a lamellar lipid bilayer, shows that the defect is unstable: defects of dimensions smaller than γ/σ spontaneously self-heal and the larger ones grow indefinitely.[4] Thus, membrane phases of single lipids at equilibrium do not exhibit stable defects.

Transiently formed defects, however, are pervasive in biological membranes as well as in many mixed lipid bilayers. In living systems, they provide a generic route for a variety of important biological processes including budding, endocytosis, viral infections, and membrane fusion, to name a few.[5] Defects also arise when cellular (or multicomponent) synthetic lipid bilayers interact with antimicrobial peptides,[6] soluble proteins,[7] detergents,[8,9] and lysolipids.[10] In the latter cases, edge is generally stabilized when the edge-energy penalties are reduced by accumulation of lipids with spontaneous curvatures (e.g., positive curvatures) or when relaxation of membrane tension becomes important. Stable edges also form when synthetic single lipid bilayers are spread on textured surfaces containing defects, or when supported lipid bilayers are

[†] Biophysics Graduate Group, University of California.
[‡] Department of Applied Science, University of California.

(1) Seifert, U.; Lipowsky, R. In *Handbook of Biological Physysics*; Lipowsky, R., Sackmann, E., Eds.; Elsevier Science: Amsterdam, 1995; Vol. 1; p 403.
(2) Tanford, C. *Science* **1978**, *200*, 1012.
(3) Helfrich, W. *Z. Naturforsch., C: J. Biosci.* **1973**, *C 28*, 693.
(4) Litster, J. D. *Phys. Lett. A* **1975**, *A 53*, 193.
(5) Chernomordik, L. V.; Kozlov, M. M. *Annu. Rev. Biochem.* **2003**, *72*, 175.
(6) Huang, H. W.; Chen, F. Y.; Lee, M. T. *Phys. Rev. Lett.* **2004**, 92.
(7) Engelman, D. M. *Science* **1996**, *274*, 1850.
(8) Kragh-Hansen, U.; le Maire, M.; Moller, J. V. *Biophys. J.* **1998**, *75*, 2932.
(9) Puech, P. H.; Borghi, N.; Karatekin, E.; Brochard-Wyart, F. *Phys. Rev. Lett.* **2003**, 90.
(10) Seeman, P. *J. Cell Biol.* **1967**, *32*, 55.

10.1021/ja100294k

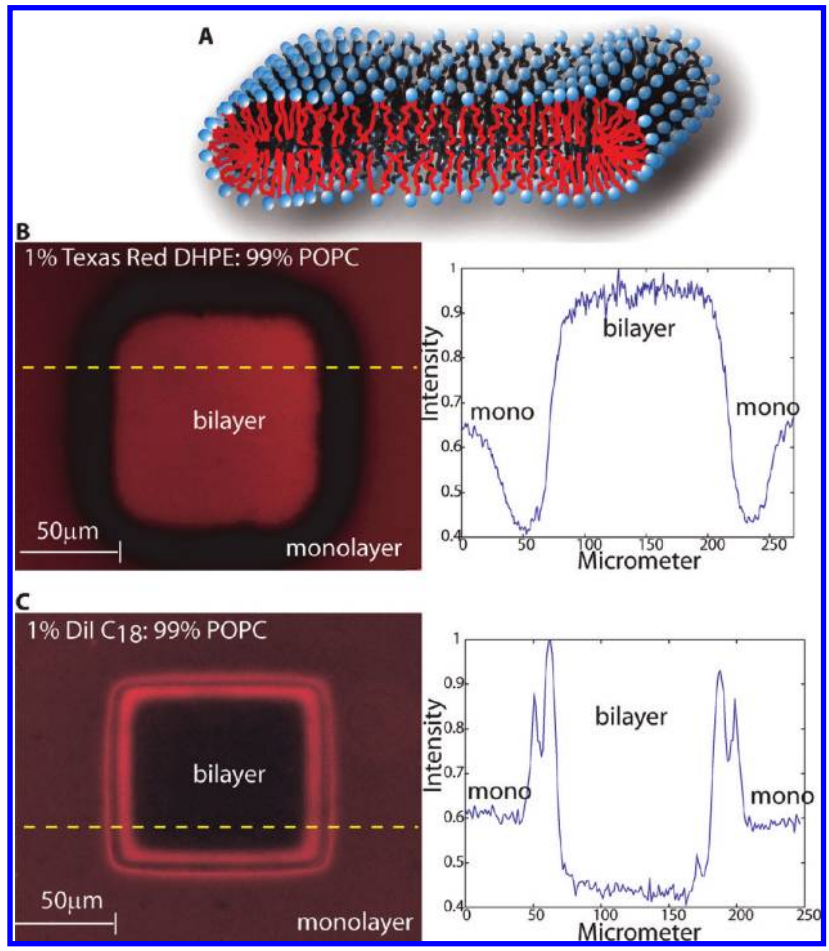

Figure 1. (A) A cartoon depiction of proposed molecular organization of lipids in a discrete bilayer patch. The cartoon highlights the proposed time-averaged organization of dense, conformationally ordered lipids within the hemi-micellar edge and its bulging effect on the surrounding bilayer microenvironment. (B) An epifluorescence image of the Texas-Red-DHPE doped 1-Palmitoyl-2-oleoyl-*sn*-glycero-3-phosphocholine (POPC) monolayer and bilayer formed on a surface with patterned *n*-octadecyltrichlorosilane (OTS) glass slides. The subsequent fluorescent intensity linescan displays a homogeneous 2-fold increase in intensity of the bilayer compared to the monolayer region which is separated by a previously characterized[27] lipophobic moat region. (C) An epifluorescence image of the POPC lipid sample with a phase sensitive dye, DiI-C_{18}, incorporated into the monolayer and bilayer region. The line profile shows an overall decrease in intensity of fluorescence in the bilayer regions compared to the surrounding monolayer region with a dramatic increase in intensity in the vicinity of the edge.

formed by vesicle fusion or Langmuir−Blodgett techniques onto patterned solid surfaces.[11,12] The stability of the edges for large bilayer patches, can be attributed to compensation of edge energy by the membrane−substrate adhesion energy.[13,14]

Regardless of the mechanism of edge formation, in all of these cases, the bilayer must remodel near the edge. This is because hydrophobic penalty associated with exposing the hydrophobic tails of the boundary lipid molecules must induce molecular reorganization.[15] In fact, previous studies suggest that the polar headgroups of the boundary lipids rearrange in a molecularly tight curved geometry connecting the two constituent leaflets of the bilayer.[4] Such a hairpin geometry constrains the acyl chains in the hemispherical or hemicylindrical configuration as illustrated in Figure 1A. At the molecular level, the appearance of such pseudomicellar motif within the lamellar bilayer configuration raises several important questions: (1) How does the self-assembly of essentially cylindrical lipids proceed within the metastable hemimicellar configurations curved at length scales comparable to molecular dimensions? (2) How does the competition between surface forces at the curved polar headgroup/water interface (e.g., dipolar repulsions and solvation forces) and those at the hydrophobic core (e.g., van der Waals, steric constraints, and *trans*−*gauche* conformational equilibria) affect the details of molecular structure within the micellar configuration? (3) Does the incipient micellar geometry induce structural change, molecular redistributions, and phase transformation in the vicinity of the defect in the lamellar bilayer? and (4) If the latter, how does the micellar edge structure spatially evolve toward the bulk-lamellar (or bilayer) motif?

Recently, there have been reports of computer simulations of molecular reorientations and attendant structural perturbations near the edge of a lipid bilayer.[16,17] These studies suggest that the energetically strained, hemimicellar edge exhibits greater chain disorder and enhancement in local dynamics than those in the lamellar bulk. Specifically, one of these studies predict that local diffusion constant within the edge is as much as 10-

(11) Groves, J. T.; Boxer, S. G. *Acc. Chem. Res.* **2002**, *35*, 149.
(12) Yee, C. K.; Amweg, M. L.; Parikh, A. N. *J. Am. Chem. Soc.* **2004**, *126*, 13962.
(13) Hamai, C.; Cremer, P. S.; Musser, S. M. *Biophys. J.* **2007**, *92*, 1988.
(14) Lipowsky, R.; Seifert, U. *Mol. Cryst. Liq. Cryst.* **1991**, *202*, 17.
(15) May, S. *Eur. Phys. J. E* **2000**, *3*, 37.
(16) Kasson, P. M.; Pande, V. S. *Biophys. J.* **2004**, *86*, 3744.
(17) Jiang, F. Y.; Bouret, Y.; Kindt, J. T. *Biophys. J.* **2004**, *87*, 182.

fold higher than in the lamellar bulk[17] fostering lipid flip-flop across the two leaflets of the bilayer. These predictions, akin to earlier "liquid hydrocarbon droplet" model[2] for micellar organization, are however inconsistent with independent simulations of lysolipid micelles.[18,19] The latter predict ordered acyl tails and even dynamic packing, characterized by rocking and rolling of lipid clusters within the micelle, dominated more by the compact packing of acyl tails rather than surface dipoles associated with the lipid head-groups. Experimental validation of these predictions is, however, still lacking.

In the work reported here, we present experimental evidence for the appearance of a unique molecular-level order in the vicinity of the bilayer's edge. Using discrete patches of substrate-supported lipid bilayers exhibiting stable edge defects, in conjunction with epifluorescence and vibrational spectroscopy measurements, we demonstrate that the bilayer structure near the edge is characterized by (1) an increase in intramolecular conformational order; (2) reduced effective lateral mobility; and (3) a distinctly higher local, effective gel-fluid transition temperature in comparison to their bulk counterpart. Together, these features signal the emergence of a distinct, ordered structural state triggered by the presence of the edge.

Materials and Methods

Materials. 1-Palmitoyl-2-oleoyl-*sn*-glycero-3-phosphocholine (POPC), 1,2-dimyristoyl-*sn*-glycero-3-phosphocholine. 1,2-dimyristoyl-*sn*-glycero-3-phosphocholine (DMPC), and 1,2-dipalmitoyl-*sn*-glycero-3-phosphocholine (DPPC) were purchase from Avanti Polar Lipids (Birmingham, AL). 1,1′-Dioctadecyl-3,3,3′,3′- tetramethylindocarbocyanine perchlorate (DiI C18) and 1,2-dihexadecanoyl-*sn*-glycero-3-phosphoethanolamine, triethylammonium salt (Texas Red DHPE) probes were purchase from Invitrogen. Hydrogen Peroxide (30% v/v) and sulfuric acid were purchases from J.T. Baker (Philipsburg, NJ) and Fisher Chemicals (Fairlawn, NJ), respectively. Octadecylitricholorosilane (OTS) 90+% was purchased from Aldrich. All organic solvents were HPLC grade. All chemicals were used without further purification. Deionized water (approximately 18.0 mΩ·cm) was obtained by processing water first through reverse osmosis deionized unit and then Milli-Q Plus water unit (Model ZD40-11595, Bedforf, MA) consisting of a five-bowl purification system (equipped with two Ion-Ex, one Super-C, one Organex-Q, and an additional ultrafiltration cartridge). Phosphate buffer saline (PBS, pH 7.2, 154 mM NaCl, 1.54 mM KH_2PO_4, and 2.71 mM Na_2HPO_4) was obtained from Gibco-Life Technology (Rockville, MD) and used as vesicle spreading solution and buffer media. Corning glass coverslips (No. 1, 1/2 mm^2, Fisher HealthCare, Houston, TX) were used as substrates. The glass substrates were cleaned from contaminants by oxidizing in a freshly prepared 4:1 (v/v) mixture of sulfuric acid and hydrogen peroxide for a period of 3 min maintained at 100 °C (Caution: this mixture reacts violently with organic materials and must be handled with extreme care). The substrates were then withdrawn using Teflon tweezers, rinsed immediately with a copious amount of deionized water, and dried in a stream of nitrogen. All cleaned, oxidized substrates were used within 4 h of the pretreatment.

Methods. 1. Substrate Preparations. The glass substrates were cleaned from contaminants by oxidizing in a freshly prepared 4:1 (v/v) mixture of sulfuric acid and hydrogen peroxide for a period of 3 min maintained at 100 °C (Caution: this mixture reacts violently with organic materials and must be handled with extreme care). The substrates were then withdrawn using Teflon tweezers, rinsed immediately with a copious amount of deionized water, and dried in a stream of nitrogen. All cleaned, oxidized substrates were used within 4 h of the pretreatment.

Supported phospholipid bilayers were formed primarily using previously reported vesicle fusion and rupture method.[20,21] Briefly, small unilamellar vesicles (SUVs) were prepared using vesicle extrusion methods.[22] Typically, a desired amount of lipid or lipid mixtures suspended in chloroform or chloroform/methanol mixtures were mixed in a glass vial. Dye concentrations were 1 mol % for stocks containing Texas or 0.5−1 mol % for $DiIC_{18}$. The solvent phase was then evaporated under a stream of nitrogen and subsequently evacuated for at least 1 h in a vacuum desiccator. The dried lipid mixture was then suspended in Millipore water and kept at 4 °C to be rehydrated overnight. The total lipid concentration was 2 mg/mL. The desired amount of hydrated aqueous solution was then sonicated and passed through a Avanti Mini-Extruder (Avanti, Alabaster, AL) using 0.1 μm polycarbonate membrane filters (Avanti, Alabaster, AL) 21 times at a desired temperature (typically 10 °C above the transition temperature). One part of the resulting SUV solutions was diluted with one part of PBS and kept above the T_m until used. Vesicles were used within a few hours of extrusion.

2. UV Photolithography of Octadecyltrichorosilane Monolayers.[23] Spatial patterning of *n*-octadecyltrichlorosilane (OTS) covered substrates was achieved using shortwavelength UV radiation.[24,25] In particular, spatially directed photoillumination of monolayer samples was achieved using a physical mask and an ozone-generating UV lamp.[26] The masks displaying patterns of chrome over quartz substrate were either acquired from Photoscience, Inc. (Torrance, CA) or produced at the UC Davis Microfabrication Facility. On selective masks, the edges of the chrome were deliberately roughened by overexposure of the protective photoresist layer prior to etching of the chrome. UV radiation was produced using a medium pressure Hg-discharge grid lamp (UVP, Inc., Upland, CA) in a quartz envelope and maintained in a closed chamber in a chemical hood. The samples were placed in contact with the photomask and positioned approximately 0.5−2 mm from the light source depending on the illumination geometry. (Caution: direct exposure to short-wavelength UV light (187−254 nm) must be avoided, and appropriate eyewear must be worn. Care must be taken in venting the ozone by operating grid lamps under chemical hoods. The breathing of ozone in high concentrations is dangerous. Ozone concentration in excess of 0.1 ppm can cause irritation.) The exposure period was approximately 40−60 min depending on the exposure geometry (sample-lamp distance) and the age of the lamp. Following the exposure, the mask was separated from the substrate surface, and samples were rinsed thoroughly using water, chloroform, and ethanol, and dried with nitrogen. Patterned OTS samples were used within 24 h of preparation.

3. Vesicle Spreading on Glass Substrates or Patterned OTS Surface. Vesicle spreading was carried out by placing either glass substrates or patterned OTS substrates over a 40 μL SUV solution drop placed at the bottom of a plastic Petri dish. The samples were allowed to incubate for 10−20 min to ensure equilibrium coverage. The Petri dish was then filled with water and transferred to a large reservoir of water in which the substrate was shaken gently to remove excess lipids. Supported bilayer samples prepared in this way were then stored in deionized water or PBS buffer for further characterization.

(18) Dill, K. A.; Flory, P. J. *Proc. Natl. Acad. Sci. U.S.A.* **1981**, *78*, 676.
(19) Wendoloski, J. J.; Kimatian, S. J.; Schutt, C. E.; Salemme, F. R. *Science* **1989**, *243*, 636.
(20) Bayerl, T. M.; Bloom, M. *Biophys. J.* **1990**, *58*, 357.
(21) Cremer, P. S.; Boxer, S. G. *J. Phys. Chem. B* **1999**, *103*, 2554.
(22) Mayer, L. D.; Hope, M. J.; Cullis, P. R. *Biochim. Biophys. Acta* **1986**, *858*, 161.
(23) Howland, M. C.; Johal, M. S.; Parikh, A. N. *Langmuir* **2005**, *21*, 10468.
(24) Dulcey, C. S.; Georger, J. H.; Krauthamer, V.; Stenger, D. A.; Fare, T. L.; Calvert, J. M. *Science* **1991**, *252*, 551.
(25) Jonas, U.; del Campo, A.; Kruger, C.; Glasser, G.; Boos, D. *Proc. Natl. Acad. Sci. U.S.A.* **2002**, *99*, 5034.
(26) Vig, J. R. *J. Vac. Sci. Technol., A* **1985**, *3*, 1027.
(27) Howland, M. C.; Sapuri-Butti, A. R.; Dixit, S. S.; Dattelbaum, A. M.; Shreve, A. P.; Parikh, A. N. *J. Am. Chem. Soc.* **2005**, *127*, 6752.

4. Epifluorescence Microscopy. A Nikon Eclipse TE2000-S inverted fluorescence microscope (Technical Instruments, Burlingame, CA) equipped with a Roper Cool Snap camera (Technical Instruments) and a Hg lamp as the light source was used to visualize all fluorescent samples. Filter cubes were used to filter absorption and emission to the source and the CCD camera, respectively. Typically, images were taken using either a Plan Fluor 10× (NA, 0.25) or a Plan Fluor, ELWD, 20× (NA 0.45) objective (Nikon, Japan). Images were stored and processed using Matlab6 and a simple PCI software (Compix, Inc., Cranberry Township, PA) augmented with a quantitative dynamic intensity analysis module. Excitation and emission maxima for the probes used were 583/601 nm for TR-DHPE and 549/564 DiI-C_{18}. Fluorescent images were taken every 2 min at 0.4−0.6 s exposure time.

5. Laser Fluorescent Recovery after Photobleaching. Laser Fluorescent Recovery After Photobleaching (FRAP) experiments were performed with a Coherent diode 532 nm laser. The laser was externally fiber coupled into a Nikon Frap Attachment that was mounted on the microscope. Photobleaching of a 10 μm^2 area of the fluorescently doped lipid bilayer was achieved using a 10× or 20× objective. Laser exposure times were 10 s at 1 mW unless otherwise noted.

6. Temperature Cycling Experiments. A heated 1% DiI C_{18}/99%DMPC extruded solution (35 °C) was allowed to incubate for 10 min on an OTS patterned slide to ensure complete coverage over the substrate. After which time, the sample was placed in a container of chilled deionized water (7 °C). This would arrest any diffusion that has already taken place over the last 10 min. The slide was then rinsed in the chilled bath to remove any unruptured vesicles then placed in a plastic Petri dish that was put on a temperature controlled stage, Bionomic BC-100 (20/20 Technology, Inc.), set for 10 °C. The temperatures recorded correspond to readings taken with a thermocouple that was placed in the sample Petri dish.

7. Bilayer Formation on Internal Reflection Element (IRE). A bilayer was formed on a plasma cleaned or phirahna etched silicon IRE via vesicle fusion method. The IRE was placed on top of 400 μL of vesicle solution and allowed to incubate for approximately 10 min before being placed in a large water bath to remove excess lipids. The IRE was then assembled inside a flow-cell under water. PBS was then flushed through the flow cell to create a buffer reservoir.

8. Attenuated Total Reflection-Fourier Transform Infrared Spectroscopy (ATR-FTIRS). ATR-FTIR was recorded using a Bruker Equinox 55 Fourier transform infrared spectrophotometer equipped with a demountable ATR flow cell. The spectra frequency range is 4000−600 cm^{-1} and obtained at 2 cm^{-1} resolution for 256 scans using a Blackman Harris 3 term apodization. The interferrograms were zero-filled to increase the point density by a factor of 16. The data analysis was performed using Grams 32 software (Galactic Industries, Salem, NH) and plotted with Matlab.

Results

We begin with the preparation of isolated patches of supported lipid bilayers displaying arrays of bilayer edges at spatially defined locations. Such a bilayer configuration is conveniently achieved by allowing small unilamellar vesicles (SUVs) to fuse and spread over surfaces displaying predetermined patterns of surface energy or wettability.[27] Specifically, we use low-energy hydrophobic substrates incorporating predetermined arrays of hydrophilic "wells" where discrete bilayers form. We use photopatterned *n*-octadecyltrichlorosilane (OTS) monolayers on glass. Preassembled OTS monolayers, prepared by following a standard solution self-assembly procedure, are subsequently exposed to an ozone generating short-wavelength ultraviolet radiation (184−257 nm) in desirable patterns using a physical photomask. The treatment results in binary patterns of surface energy comprising oxidized silica in the UV-exposed regions (hydrophilic wells) surrounded by a uniform hydrophobic background consisting of intact OTS in UV-protected regions (hydrophobic). Subsequently, these substrates are exposed to aqueous dispersions of SUVs (hydrodynamic diameter of ∼100 nm), consisting of a single phospholipid, 1,2-dimyristoyl-*sn*-glycero-3-phosphocholine (DMPC; T_m, 24 °C). To enable fluorescence-based characterization and also to discriminate between any co-existing phases, the bilayers are doped with small amounts of fluorescent lipid analogues. We doped the DMPC bilayers with DiI-C_{18} (1,1′-dioctadecyl-3,3,3′,3′-tetramethylindocarbocyanine perchlorate; 1 mol %) or Texas Red 1,2-dihexadecanoyl-*sn*-glycero-3-phosphoethanolamine triethylammonium salt (TR-DHPE, 1 mol %). The long-chain DiI-C_{18} lipid probe, consisting of a large indocarbocyanine headgroup and two octadecyl chains, inserts itself into the bilayer with its headgroup roughly perpendicular to the plane of the bilayer. The slightly longer alkyl chains (C_{18}) compared to the host DMPC acyl chains (C_{14}) result in a strong preferential association of the probe with ordered conformers (typically associated with gel like bilayer states) in the bilayer.[28] The substrate pattern of wettability directs vesicle fusion, giving rise to spontaneous corralling of single fluid lipid bilayers from the surrounding fluid monolayers by a lipid-free transition region. This approach produces a high-density of well-defined edges of confined bilayer patches in a spatially predetermined fashion.[27]

Initial evidence for the appearance of a unique molecular order near the membrane edge is provided by a striking fluorescence pattern observed for DMPC bilayers doped with the gel-partitioning DiI-C_{18} probe (Figure 1C). Similar patterns were also observed for DiI-C_{18} doped POPC and DPPC bilayers (Supporting Information). This unique fluorescence profile is in sharp contrast to an essentially uniform fluorescence emission observed routinely for DMPC bilayers (Figure 1B) doped with trace concentrations of Texas-red DHPE or other phase-insensitive probes (e.g., NBD-PE). As seen in epifluorescence images and corresponding line scans for DiI-C_{18} doped DMPC bilayers (Figure 1C), the compartmentalized bilayer, namely, the square elements in Figure 1, is brightly lit in the vicinity of the edge with the two-dimensional (2D) bulk of the bilayer interior emitting a low but homogeneous fluorescence intensity. Note that in both samples (Figure 1B,C), the fluorescent areas surrounding the bilayer patch are DMPC monolayers that have formed on the hydrophobic regions of the patterned substrate. The presence of essentially fluorescence-free "moat" region lends additional confidence that the two, mono- and bilayer regions, are separated (see above) and that the fluorescence behavior of the bilayer element (square-shaped region) is not influenced by the surrounding monolayer phase. The linescan image (Figure 1C) shows that the DiI-C_{18} probe also concentrates at the periphery of the lipid monolayer as indicated by the presence of two peaks, one due to the bilayer and the other due to the monolayer. While the accumulation of the DiI-C_{18} probe near monolayer boundary is interesting in its own right, we limit our attention to the edge of the discrete (square-shaped) bilayers.

This nonuniform DiI-C_{18} distribution suggests the presence of co-existing and distinctly different molecular environments within the bilayer patch. Since DiI-C_{18} is known to preferentially partition with conformationally ordered lipids (see above), its

(28) Spink, C. H.; Yeager, M. D.; Feigenson, G. W. *Biochim. Biophys. Acta* **1990**, *1023*, 25.

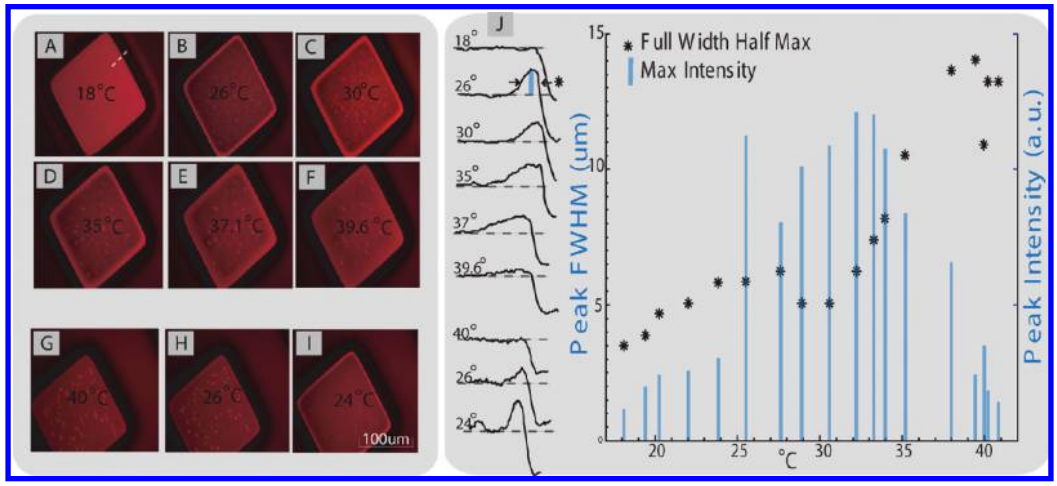

Figure 2. (A−H) A sequence of epifluorescence images of a 1,2-dimyristoyl-*sn*-glycero-3-phosphocholine (DMPC) bilayer patch undergoing a heating\cooling cycle between 18 and 40 °C. (J) Corresponding linescans delineating the temperature dependence of the spatial variations of intensity in the vicinity of a bilayer edge. (J) A plot of full width half maxima (fwhm) of the characteristic peak intensity peak and intensity height versus temperature. This demonstrates first the preference and eventual accumulation of dye molecules at the bilayer edge after a patterned bilayer sample is heated above the T_m of DMPC (26 °C) with maximum preference at 26 °C corresponding to maximum intensity.

increased fluorescence emission near the edge is consistent with the presence of a dense gel-like lipid microenvironment there. Because the precise value of the emission intensity of DiI-C_{18} is strongly dependent on its lipid microenvironment, and our wide-field measurements have limited spatial resolutions (1−2 μm), quantifying partitioning preference or the width of perturbed membrane near the edge is not possible from our data alone. Nevertheless, such an accumulation of ordered conformers near the edge suggests denser packing and a distinctly different molecular organization.

To further corroborate that the enhanced fluorescence intensity due to DiI-C_{18} observed near the bilayer edges indeed documents the presence of a denser local lipid microenvironment, we thermally modulate the bilayer phase and monitor the temperature-dependent dye redistributions. The temperature of the DMPC bilayers doped with DiI-C_{18} is first lowered to 18 °C, well-below DMPC T_m (24 °C). Subsequently, the sample is allowed to equilibrate at several arbitrarily selected temperatures between 18 and 40 °C in a slow heating−cooling cycle and their temperature-dependent fluorescence images are recorded. These data, summarized in Figure 2 (complete linescans in Supporting Information), demonstrate fully reversible temperature-dependent fluorescence intensity redistributions. At the lowest equilibrated temperature, ∼18 °C, the fluorescence intensity is essentially homogeneous across the bilayer patch. This absence of edge-preference by DiI-C_{18} (see above) is not surprising because at this temperature the bulk of the bilayer is gel-like and matches the phase state near the edge as inferred above. As the sample temperature is raised to above the DMPC transition temperature (T_m), a bright and narrow rim reemerges, such as observed for room-temperature prepared samples as in Figure 1. This is consistent with the appearance of co-existing phases wherein the bulk of the bilayer is fluidized whereas the bilayer near the edge retains its gel-like character. As the temperature is raised even further, the bright rim near the edge widens further suggesting a gradual diminution of the DiI-C_{18}'s preference for localization near the edge, which ultimately vanishes producing a uniformly fluorescent bilayer at ∼40 °C. This high temperature fluorescence homogenization is now consistent with a uniform fluid phase expected for both the edge and the bulk regions of the bilayer. It is notable that the narrowest width for the fluorescent rim is observed at temperatures near, but slightly larger, than the T_m. Upon re-equilibrating the samples at a series of temperatures during a cooling cycle, the fluorescence contrast pattern gradually reappears (Figure 2) as the uniform fluid phase is replaced by the formation of the gel-like edge. This fully reversible temperature dependent spatial reorganization of DiI-C_{18} within the bilayer is fully reproducible in multiple thermal cycles and across multiple independent samples.

There are three key noteworthy features in these data. These observations of directed, temperature-dependent DiI-C_{18} redistribution within the bilayer establish that the observed preference of DiI-C_{18} for the edge of the bilayer is not a kinetic artifact dependent on the sample preparation or the thermal history of the sample. Rather they show that the distribution of the probe across single contiguous patches of bilayers depends on the sample temperature and phase state of the bulk of the bilayer, and that it can be fully reversed by thermally modulating the bilayer environment. On the basis of this reversibility, we can rule out any substantial pinning of DiI-C_{18} at the membrane periphery. Additionally, the appearance of narrow width of bright fluorescent rim near the bulk (DMPC) T_m is entirely consistent with a scenario wherein the bulk of the bilayer undergoes the expected thermotropic gel−liquid crystalline phase transition, whereas the narrow rim in the vicinity of the physical edge of the bilayer remains in its low temperature gel phase even above the bulk T_m. At higher temperature, widening of the fluorescent rim signals the loss of DiI-C_{18}'s preference for the region near the edge suggesting that the lipid microenvironment near the edge must begin to melt and fluidize. The ultimate reemergence of a uniform fluorescence at temperatures above ∼40 °C suggests the appearance of single homogeneous fluid state and places the upper threshold for the temperature at which complete lateral fluidity is established across the entire bilayer patch. Lastly, the gradual temperature-dependent widening of the fluorescent rim also suggests that, at temperatures above bulk T_m (∼24 °C) and below 40 °C, the gel-like state near the edge and the fluid state in the bulk of the bilayer is not separated by a sharp physical boundary. Curiously, a broad region of physical state intermediate between the gel-like boundary region and the fluid bulk characterizes the boundary.

The presence of gel-like regions above the bulk T_m of the lipid in the vicinity of the edge inferred above raises a relevant

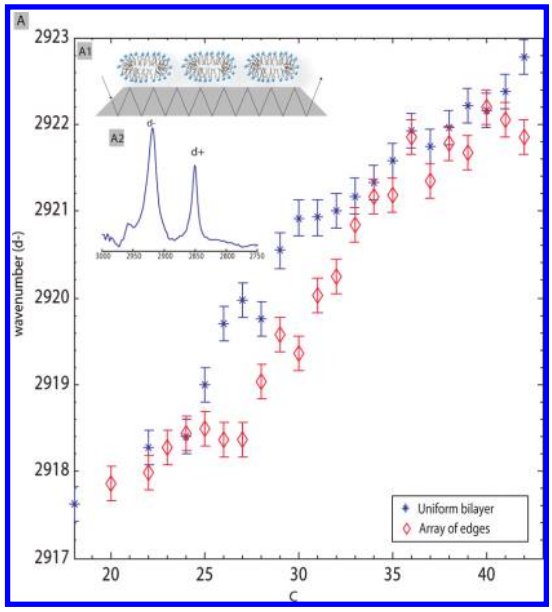

Figure 3. A comparison of the temperature dependence of attenuated total reflected Fourier transform infrared (ATR-FTIR) spectra of a continuous DMPC bilayer and a DMPC bilayer displaying multiple edges formed by UV patterning. (A1) An schematic illustration of a patterned bilayer formed on a ATR-FTIR crystal and (A2) a representative example of a typical spectrum. (A) Position of conformationally sensitive symmetric methylene stretching (d^-) absorption peak plotted with respect to temperature for a plain DMPC bilayer and a patterned DMPC bilayer displaying a high-density of edges.

question: is the region near the edge characterized by the sustained presence of ordered *trans* conformers? To address this question, we performed independent attenuated total reflection Fourier-transform infrared (ATR-FTIR) spectroscopy measurements (Figure 3). ATR-FTIR traces of DMPC bilayer samples displaying a high-density spatial array of edges, created by UV-photolithography (schematic Figure 3A1), are recorded as a function of temperature over a thermal cycle spanning the T_m over the same temperature range as above. For comparison, uniform single bilayers (which do not contain engineered edges) are also examined. A representative spectrum in the 2700−3100 cm^{-1} frequency region is shown in Figure 3A2. The spectrum is characterized by the presence of a number of overlapping peaks with immediately discernible maxima at 2850, 2919, and 2956 cm^{-1}, which can be straightforwardly assigned to primary contributions from the methylene C−H symmetric (d^+) and antisymmetric (d^-) stretching modes and the methyl C−H antisymmetric stretching modes, respectively. The two dominant methylene stretching mode absorption peaks observed at ∼2850 cm^{-1} (d^+) and ∼2918 cm^{-1} (d^-) are well-known diagnostic markers for the temperature dependent changes in the average chain conformational order:[29] the peak frequencies of these vibrational modes are typically reported to lie in the narrow ranges of 2848−2850 cm^{-1} (d^+) and 2916−2918 cm^{-1} (d^-) for *all-trans* extended chains and in the distinctly different ranges of 2854−2856 cm^{-1} and 2924−2928 cm^{-1} for conformationally disordered chains in fluid lipids, characterized by a dominant presence of gauche conformers. Intermediate values for these two peaks then either represent a mixed population consisting of ordered and disordered chains or suggest the presence of partially ordered chains. On this basis, it is instructive to compare the temperature-dependent positions of the two peaks for the edge-displaying and uniform bilayer samples. This comparison is illustrated in Figure 3A for d^+ methylene peak (d^- in Supporting Information). The plot clearly reveals that both samples undergo order−disorder transition between ∼25 and ∼35 °C. A closer inspection reveals that, at all temperatures between 25 and 35 °C, the peak positions are systematically lower for samples containing many edges. This in turn indicates that the average density of ordered conformers is measurably higher for edge-displaying samples relative to single contiguous ones. Note that the observed positions of the peaks represent averages due to the conformers near the edge as well as those in the bulk of the bilayer. These observations of increased ordered conformers in edge-displaying samples are consistent with the foregoing inference that regions near the edges retain nonfluid gel-like state at temperatures above T_m. They further suggest that these regions are not molecularly disordered but dense amorphous regions, but appear to be characterized by ordered dense regions.

Lateral fluidity is an intrinsic property of lipid bilayers with important biophysical consequences.[30−32] It is also linked to the highly cooperative lipid phase transitions.[33] To determine how the presence of gradient of ordered conformers near the bilayer edge alters the local diffusional characteristics and phase behavior, we adapted the classical fluorescence photobleach recovery (FRAP) measurement. A typical FRAP experiment[34] involves the photobleaching of a geometrically defined spot within the bilayer medium at a given temperature and monitoring the time-dependent recovery. The rate of fluorescence recovery measures the lateral diffusion of the probe and hence the fluidity of the medium. In our adaptation of this technique, we probe the temperature-dependent onset of lateral mobility, which we refer to as fluidity transition temperature (T_{ft}), as the temperature at which the photobleached spot begins to diffuse as the supported bilayer undergoes gel to fluid transition. By spatially varying the position of the spot on the bilayer, a map of local fluidity transition temperatures can be easily generated. In the experiment illustrated in Figure 4, the temperature of the bilayer is first lowered to ∼8 °C, a temperature value below the T_m (or premelting) transition temperature. Two microscopic spots (5 μm diameter) are then photobleached in the DMPC bilayer (doped with 1 mol % Texas-red-DHPE dye). The spatial locations of the two spots are chosen such that one spot is bleached deep within the interior of an isolated bilayer patch and the second is near the bilayer edge. Subsequently, the temperature-dependent evolution of the photobleached spot is monitored during a slow heating cycle (0.1 °C/min). We used Texas Red DHPE, a probe which does not show preference for the edge or the bulk of the bilayer, as the fluorescent probe (see Figure 1A) for the temperature-dependent FRAP measurements. This is to avoid complications (compositional gradients) arising from the use of phase-sensitive dyes (e.g., DiI-C_{18}). Figure 4 shows selected frames from a typical sequence of fluorescence images obtained at several arbitrarily chosen temperatures during our temperature-dependent FRAP experiment. These images confirm that the photobleached spot begins

(29) Casal, H. L.; Mantsch, H. H. *Biochim. Biophys. Acta* **1984**, *779*, 381.
(30) Jacobson, K.; Sheets, E. D.; Simson, R. *Science* **1995**, *268*, 1441.
(31) Vaz, W. L. C.; Goodsaidzalduondo, F.; Jacobson, K. *FEBS Lett.* **1984**, *174*, 199.
(32) Vereb, G.; Szollosi, J.; Matko, J.; Nagy, P.; Farkas, T.; Vigh, L.; Matyus, L.; Waldmann, T. A.; Damjanovich, S. *Proc. Natl. Acad. Sci. U.S.A.* **2003**, *100*, 8053.
(33) Jorgensen, K.; Mouritsen, O. G. *Thermochim. Acta* **1999**, *328*, 81.
(34) Axelrod, D.; Koppel, D. E.; Schlessinger, J.; Elson, E.; Webb, W. W. *Biophys. J.* **1976**, *16*, 1055.

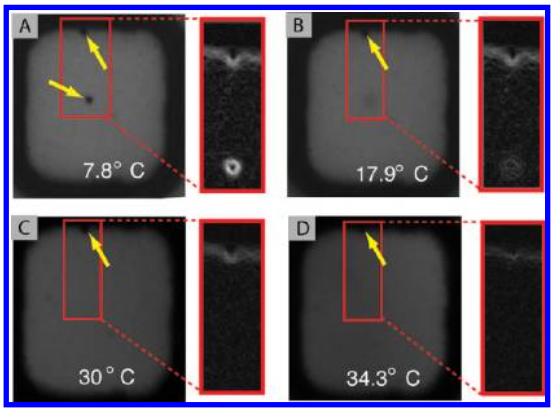

Figure 4. (A) Initial epiflourence image of photobleached spots at the center of the bilayer and edge of a DMPC bilayer at 7.8 °C. Arrows highlight the position of the photobleached spots. (B) Epifluorescent image of bilayer at 17.9 °C displaying a blurring of the photobleached spot at the center while the edge spot remains unchanged. (C) Temperature is raised until 30 °C, well above the T_m of DMPC, revealing complete recovery of the photobleached spot in the center and the apparent unperturbed photobleached area at the edge. (D) Final epifluorencent image taken at 34.3 °C showing the fluorescent recovery of the photobleach spot at the edge of the bilayer.

to blur, indicating the onset of lateral diffusion at roughly 24 °C, for the spot near the center of the bilayer patch, in good correspondence with the bulk transition temperature T_m. In a dramatic contrast, the photobleached spot near the edge retains its shape up to 38 °C, at which temperature the spot begins to lose its definition. This simple experiment unambiguously establishes that the onset of lateral fluidity or the T_{ft} near the edge is delayed in temperature by as much as 14 °C, suggesting a significantly higher local *"equivalent transition temperature"* for the bilayer near the edge.

Discussion

Structural Summary. Many previous studies have postulated the organization of lipids into a hemimicellar structure near the edge. While our studies cannot directly provide characterization of the edge alone, they offer insight into structural deformations that occur in the vicinity of the edge. Our results provide strong evidence that the presence of an edge (or a topological defect) induces a peculiar molecular organization in its vicinity. Key features of this organization include (1) a net increase in intramolecular acyl-chain conformational order; (2) increase in intermolecular packing density; (3) lowered effective lateral mobilities near the edge; (4) an elevated effective temperature for the onset of lateral fluidity near the edge during gel-fluid transition of the bilayer; and (5) a gradual and continuous structural transformation from the edge toward the bulk.

Evidence for an increase in chain conformational ordering relative to the bulk of the bilayer due to the presence of the edge is most directly furnished by FTIR measurements (Figure 3). Accumulation of DiI-C_{18}, which prefers molecularly ordered gel-like environment seen in data presented in Figure 1 lends further credence. This increase in intramolecular conformational order is also attended by an increase in intermolecular packing density. We have three parallel lines of evidence for edge-induced changes in the packing density. First, temperature-induced redistribution of the probe detailed in Figure 2 shows reversible accumulation of DiI-C_{18} in a narrow rim near the edge at all temperatures below 38 °C. Because DiI-C_{18} has an affinity for molecularly ordered gel-like dense phases, we can infer an increase in molecular density. Second, FTIR spectroscopy data (Figure 3) reveal that the conformation of the average chain in edge-laden samples at all temperatures between 25 and 38 °C shifts to more ordered states relative to the unpatterned bilayer. This reduction in the *gauche* population is consistent with tighter packing of the acyl tails, thus, suggesting increased molecular density. Third, we find that in our temperature-dependent FRAP measurements (Figure 4) the onset of long-range lateral fluidity occurs at considerably higher (by 14 °C) temperature than the bulk of the sample. This elevation in local transition temperature is also consistent with higher packing of the molecules in the vicinity of the edge. Increased molecular density usually corresponds to increased physical and optical thicknesses of the bilayer. Our attempts at demonstrating the increase in molecular density near the edge using ellipsometric or AFM data proved inconclusive (data not shown) due to difficulties in measuring large areas (several micrometers) consistently while maintaining angstrom level sufficient resolution using AFM and the lack of lateral resolution needed for ellipsometric determination.

Furthermore, these structural alterations in inter- and intramolecular chain ordering in edge-laden samples have consequences for the lateral fluidity. Our temperature dependent DiI-C_{18} redistributions (Figure 1) and temperature-programmed FRAP measurements (Figure 4) document these changes. These results establish that the temperature at which long-range lateral fluidity is locally enhanced in the vicinity of the edge suggests the reduction in translational mobilities of probe molecules above T_m (24 °C) and below 38 °C. The latter value represents the temperature at which preference of DiI-C_{18} for the edge is lost and long-range fluidity restored across the entire sample.

Implications for Mechanisms. Salient points brought out by the results presented here have at least threefold implications for the mechanisms by which edges might be stabilized in bilayers. These are discussed below.

First, how do essentially cylindrical lipid molecules (intrinsic curvature $C_o \sim 0$) allow the formation of pseudomicellar organization near lamellar edges? The micellar organization in heterogonous lamellar membranes is generally stabilized by edge-active molecules (e.g., lysolipids or fatty acids) that concentrate near the edge and thereby lower the line tension penalty.[15] It is likely that synthetic lipids used in the present study (~99% purity) contain a small proportion of fatty acids or partially hydrolyzed lyso-lipid (~1%) molecules. At present, we cannot rule out the accumulation of such "edge-active impurities" near the bilayer boundary. However, it appears unlikely that edges are composed entirely of such impurity molecules alone given their stable formation in vastly different samples at very high-densities. Unfortunately, determining the chemical composition within the edge is experimentally challenging. Recent reports of nanoscale resolution in mass spectrometric imaging should enable such measurements in the future.[35]

Regardless of the exact chemical composition of the edge, the configurations of the acyl tails within the hemimicellar edge are obviously constrained. Indeed, the question of surfactant and lipid organization in nonplanar amphiphilic microphases (e.g., discrete micelles) has been debated for many years, leading to many differing interpretations of experimental data.[36] The requirements of the formation of a continuous hydrophilic barrier at the hemimicellar periphery and of uniform filling of its central

(35) Kraft, M. L.; Weber, P. K.; Longo, M. L.; Hutcheon, I. D.; Boxer, S. G. *Science* **2006**, *313*, 1948.
(36) Nagarajan, R.; Ruckenstein, E. *Langmuir* **1991**, *7*, 2934.

core impose additional constraints on the lipid assembly at the edge. The latter is governed by the balance of headgroup−headgroup interactions (e.g., dipolar repulsion and solvation forces) and van der Waals forces between the neighboring chains. Using mean-field descriptions within the framework of statistical thermodynamics, Dill and Flory[18] estimate that these constraints gives rise to a unique lipid structure, characterized by a gradient of decreasing disorder (namely, *gauche* conformers) from the lipid−water interface toward the center of the micelle, challenging the long-held "liquid hydrocarbon droplet" model.[2] More recent refinements of this *static* model provided by molecular simulations of a lysolipid micelle,[19] explicitly accounting for the headgroup solvation forces, reveal a *dynamic* picture. Here, the micelle structure reveals that the lipids are organized as clusters consisting of conformationally ordered acyl tails, which produce a continuous hydrophilic barrier at the headgroup interface by executing "rocking and rolling" motion relative to one another. The lack of resolution in experimental methods do not allow direct measurements of these edge properties, but the evidence for increase in chain conformational order as well as of denser local packing near the edges in edge-displaying samples lend indirect support to this picture.

Second, our results indicate that the edge-induced bilayer deformation is characterized by (1) a sustained gradient of increasing chain conformational order; (2) reduced long-range lateral mobilities; and (3) elevated effective transition temperatures. These observations point to a gradual and continuous spatial progression of the hemimicellar structure at the bilayer edge toward the lamellar bulk. While we could not ascertain the precise length scale over which the hemimicelle to planar structural transition occurs within the bilayers, we find that the extent of this perturbation to the bilayer planarity is strongly temperature dependent. Specifically, the presence of narrow rim near the bulk T_m is consistent with localized perturbation. At elevated temperatures, the rim is wider consistent with larger length scale over which edge remodels the membrane. Near ∼38 °C, when the fluorescent probe loses its preference for the rim altogether and close to temperatures at which fluorescence becomes homogeneous, the fluorescence heoerogeniety is spread over large, macroscopic distances within the bilayer patch. We thus speculate that near this temperature, when edge also fluidizes, the bilayer is most deformed.

Likening the hemimicellar edge to embedded defects within the bilayers, it appears instructive to relate the consequences of membrane remodeling induced by the edge with the distortions induced by the presence of inclusions (e.g., transmembrane proteins) in bilayers.[37−39] The hydrophobic part of the inclusions can be either thicker or thinner than the equilibrium, unperturbed thickness of the bilayer's central core. Depending on the nature and the degree of this hydrophobic mismatch, the surrounding membrane may stretch or thin and bend producing a sustained distortion around the inclusion boundary.[40,41] In our case, the geometric constraints of the micellar-edge and the attendant chain straightening (see above) should result in an increase in the bilayer thickness near the edge. Indeed, previous molecular simulation experiments predict such thickening in bilayers near the edge.[17] Experiments using atomic force microscopy were unable to confirm such thickening probably because of inherent difficulties in such measurements in fluid ambients and possibly due to limited thickness resolution in our experimental configuration. Furthermore, previous theoretical studies estimate that, depending on the bilayer's mechanical properties, namely, bending and stretching moduli, the spontaneous curvature of the lipids, and the size and dimensionality of the inclusion object, the perturbations of the membrane may decay to unperturbed bilayer thickness over large, yet nanoscopic, distances on the range of several bilayer thicknesses.[37] While our measurements do not permit quantitative estimates for these small length scales, they nevertheless reveal that, in the vicinity of edge fluidization temperature, the perturbations persists over considerably larger distances.

Third, our observations of the existence of rims, consisting of ordered lipid conformers exhibiting reduced lateral mobilities, in the vicinity of the membrane edge may also explain how patterned supported bilayers are able to remain fixed in shape and location while retaining their spatial fidelity (see Supporting Information). They may also be relevant in understanding many important classes of dynamics associated with stable or transiently formed membrane pores and defects, whose walls share the common structural motif, namely, the micellar organization. For instance, in interpreting bulk experimental results for flip-flop dynamics[42] across the two leaflets, the presence of the ordered and less diffusive periphery near the edge suggests that the rates at which lipids diffuse toward or away from the edge may play a more important role than thought previously. In a similar vein, the mechanism for the interactions of peptides, detergent action, and fusion-pore formation may also be better understood by taking into account membrane distortions around the pores.

Acknowledgment. We thank S. Dixit, T. Allen, and S. Sherlock for discussions and correspondence. This material is based on work supported by the U.S. Department of Energy, Office of Basic Energy Sciences, Division of Materials Sciences and Engineering under Award No. (DE-FG02-04ER46173). Student support from NSF Center for Biophotonics Science & Technology for A.M.S. is gratefully acknowledged.

Supporting Information Available: Results from control experiments, as noted in the text, are presented as a series of figures and captions. This material is available free of charge via the Internet at http://pubs.acs.org.

JA100294K

(37) ArandaEspinoza, H.; Berman, A.; Dan, N.; Pincus, P.; Safran, S. *Biophys. J.* **1996**, *71*, 648.
(38) Harroun, T. A.; Heller, W. T.; Weiss, T. M.; Yang, L.; Huang, H. W. *Biophys. J.* **1999**, *76*, 3176.
(39) Koltover, I.; Radler, J. O.; Safinya, C. R. *Phys. Rev. Lett.* **1999**, *82*, 1991.
(40) Jensen, M. O.; Mouritsen, O. G. *Biochim. Biophys. Acta, Biomemb.* **2004**, *1666*, 205.
(41) Mouritsen, O. G.; Bloom, M. *Annu. Rev. Biophys. Biomol. Struct.* **1993**, *22*, 145.
(42) Kornberg, R. D.; McConnell, H. M. *Proc. Natl. Acad. Sci. U.S.A.* **1971**, *68*, 2564.